Detailed phylogenetic analysis of SARS-CoV-2 reveals latent capacity to bind human ACE2 receptor

Erin Brintnell[1+], Mehul Gupta[1+], and Dave W Anderson[1,2*]

[1]Department of Biochemistry and Molecular Biology, Cumming School of Medicine, University of Calgary

[2]Alberta Children's Hospital Research Institute, University of Calgary

[+]Co-first authors

[*]Corresponding Author:

3330 Hospital Dr NW

Calgary, AB, Canada

T2N 4N1

403-220-5646

david.anderson1@ucalgary.ca

Abstract:

SARS-CoV-2 is a once-in-a-century pandemic, having emerged suddenly as a highly infectious viral pathogen. Previous phylogenetic analyses show its closest known evolutionary relative to be a virus isolated from bats (RaTG13), with a common assumption that SARS-CoV-2 evolved from a zoonotic ancestor via recent genetic changes (likely in the Spike protein receptor binding domain – or RBD) that enabled it to infect humans. We used detailed phylogenetic analysis, ancestral sequence reconstruction, and molecular dynamics simulations to examine the Spike-RBD's functional evolution, finding to our surprise that it has likely possessed high affinity for human cell targets since at least 2013.

Main Text:

Viral pathogens are a continuous and evolving challenge for human populations.[1,2] Most known viruses maintain species-specific infectivity, often co-evolving with their host to mirror animal species trees.[3,4] While less common, the emergence of novel viral pathogens is of particular interest because they often exhibit abnormal degrees of infectivity and/or virulence,[5] having not evolved to a natural selection balance with their new host.[6] Viruses of animal origin include periodic Ebola outbreaks,[7] the 1918 "Spanish Flu",[8] and most recently, SARS-CoV-2, the viral agent that causes COVID-19.[9] In these cases, viruses spread through human populations after evolving to "cross the species barrier".[10] Yet, many questions remain for viruses of non-human origin: How do they acquire the ability to infect humans? Is it wholly dependent on "recognition" (a function typically mediated by protein-protein binding between viral capsid and target host cell), or must there be changes in other viral replication mechanisms as well? And specifically focusing on SARS-Cov-2, did it evolve to infect humans via many evolutionary changes or only a few? Was it dependent on a key functional shift in its ability to bind human cells, or is there evidence that other genomic changes were needed for it to acquire its strikingly high degree of infectivity? Answering these questions is critical if we are to understand both the origin of specific viruses, such as SARS-CoV-2, as well as the capacity of animal viruses to evolve human infectivity.

SARS-CoV-2 emerged in late 2019[11] and has high infectivity, spreading rapidly around the world, causing a global health emergency.[12] A member of the Coronaviridae family of polymorphic, enveloped, single stranded RNA viruses,[13] it is thought that SARS-CoV-2 evolved from a zoonotic origin,[14,15] owing to its clear evolutionary relationship with coronaviruses that have been isolated from animals[16] (its closest known evolutionary relative is the bat coronavirus, RaTG13[17–20] and the second-closest known relative is a pangolin coronavirus, Pangolin-CoV).[21] While most of the SARS-CoV-2 genome is most similar to the RaTG13 genome, some genomic regions, including the Spike glycoprotein Receptor Binding Domain (RBD) (which mediates viral entry into host cells), have greater sequence similarity to the Pangolin-CoV homolog,[22] prompting some to suggest SARS-CoV-2 may be the product of recombination during co-infection.[21–24]

The Spike protein is a key component of the SARS-CoV-2 infection pathway.[25] Knockout and overexpression studies have demonstrated that binding of the Spike-RBD to human angiotensin converting enzyme 2 (hACE2) mediates cellular entry of SARS-CoV-2.[26–30] The protein sequence of this surface receptor is variable, with particular rare variants increasing patient susceptibility to SARS-CoV-2 infection.[31] The SARS-CoV-2 Spike protein has been shown to bind the hACE2 receptor with greater affinity than the SARS-CoV-1 homolog, which has been suggested as a possible explanation for its greater infectivity.[29] Additionally, many other related coronaviruses have been shown to be unable to bind hACE2 with sufficient affinity to support infection, raising the possibility that high hACE2 is a recently acquired trait for SARS-CoV-2.[32–34] Given this, a critical question remains to be answered: How and when did the SARS-CoV-2 Spike protein evolve its relatively higher affinity for the hACE2?

With this question in mind, we set out to robustly characterize the evolutionary changes that accompanied the emergence of SARS-CoV-2, and that distinguish it from its closest zoonotic relatives. We focused on the evolution of the Spike-RBD by leveraging its known evolutionary

relationships to other animal and human viruses and employed ancestral sequence reconstruction in conjunction with molecular dynamics simulations to identify biochemical and biophysical changes that enhanced Spike binding to the hACE2 receptor.

Our initial phylogenetic analysis utilized whole viral genomic data, and generally supports prior studies' conclusions, finding similar levels of nucleotide identity to the RaTG13 genome (96.0% sequence identity) and the Pangolin-CoV genome (90.0% sequence identity) (**Supplementary Figure 1A**).[21,29] We next quantified the degree of evolutionary diversification that has occurred during SARS-CoV-2's global spread. We performed an in-depth analysis of 479 sequences collected between December 30, 2019 and March 20, 2020, and observe 16 polymorphisms, including 11 missense mutations present in >5% of infections (**Supplemental Table 1**), each mapping to unique phylogenetic branches (**Figure 1A**). One monophyletic clade was primarily isolated within the United States and Canada, and is defined by two synapomorphic missense mutations: c.17848A>G and c.28134C>T.[35] Since these occur in one of the most variable parts of the coronavirus genome, it is likely that its distribution is due to a founder effect and that it does not confer an evolutionary advantage.[36] It is also worth noting that neither appears in the Spike protein-coding region, making it unlikely to impact hACE2 affinity.

We subsequently sought to investigate the evolution of SARS-CoV-2 infectivity by performing ancestral sequence reconstruction for the Spike-RBD amino acid sequence (**Figure 1B**). While cross-species protein sequence comparisons have been used to investigate critical amino acid changes in the SARS-CoV-2 Spike protein,[37] leveraging the phylogenetic relationships allows us to infer the most likely ancestral sequences for this protein allows us to focus on the subset of genetic changes that are specific to its recent evolution.[38] We inferred statistically well-supported reconstructions of the Spike-RBD sequence for both the common ancestor of all human SARS-CoV-2 cases (labelled "N1", **Figure 1B,D**) and the its common ancestor with the closest animal virus (labelled "N0", **Figure 1B,D**). N1 is identical to the Spike-RBD in the SARS-CoV-2 reference sequence, as expected, while the N0 Spike-RBD sequence is, to our knowledge, unique, reflecting the uniqueness of SARS-CoV-2's viral origin.[21,39] N0 differs from N1 at 4 positions (346, 372, 498, and 519 – **Figure 1C**). The reconstruction of N1 for each of those positions is statistically well-supported, with a posterior probability (P.P.) of 1 obtained from two independent calculations (**Supplemental Table 2; Supplementary Methods**). The reconstruction for N0 has high statistical support for positions 346, 372, and 519 (P.P. > 0.94), while position 498 was ambiguously reconstructed, with two alternate states comparably probable (**Supplemental Table 2**). Together, these four changes (t346R, t372A, h/y498Q, and n519H) differentiate the evolved SARS-Cov-2 Spike protein from the most recent common ancestor with animal viruses (**Figure 1B**). As such, this ancestral virus must have existed at least as early as 2013 (as one of its descendants – RaTG13 – was isolated in that year), meaning that the branch between the N0 and N1 ancestors covers at least 7 years of molecular evolution (**Figure 1B**).

To quantify functional differences between the N0 ancestor and the Spike-RBD sequences, we conducted 10 ns molecular dynamics simulations (see **Supplementary Methods**) of the Spike Receptor Binding Domain (RBD) in complex with hACE2 (starting point for each simulation was modelled off crystal structures of the SARS-Cov2 Spike-RBD/hACE2 complex),[27] which we used

to calculate the free energy contributions from electrostatics, polar solvation, van Der Waals interactions, and solvent-accessible surface area (SASA) to infer the free energy of binding between those two proteins.[40,41] We quantified the root-mean-squared deviation (RMSD) of the portion of the RBD closest to the hACE2 receptor (residues 397 to 512) for each of our replicates to confirm complex stability (**Supplementary Figure 2**). Contrary to our expectations, the free energy of binding between the Spike-RBD and the hACE2 appears to have decreased between N0 and N1. In fact, each of the 4 changes either reduced or did not significantly change the free energy of binding (**Figure 2A**) (this is true for both alternate reconstructions of position 498 in N0). While this was somewhat surprising, it corresponds with recently released *in vitro* binding measurements remarkably.[42] In particular, we see that both alternative reconstructed states for position 498 in N0 clearly improve hACE2 binding affinity in both our simulations and in *in vitro* functional measurements.[42]

While overall it is clear these four historical changes reduced binding affinity to hACE2, they did not do so equally: t346R and h/y498Q showed the largest decreases in affinity (**Figure 2B**). These results demonstrate that, contrary to expectations, evolutionary changes since 2013 did not improve the SARS-Cov2 Spike-RBD's binding with hACE2. To our knowledge, this is the first demonstration that the SARS-CoV-2's common ancestor with the RaTG13 lineage may have been capable of binding to hACE2. This has important implications for our understanding of how SARS-CoV-2 evolved to infect humans. First, it suggests that the binding affinity between the Spike-RBD and hACE2 may not be a critical driver of the high degree of infectivity that has been observed during its recent outbreak. Instead, it suggests that tight hACE2 binding may be a latent property of this virus, and that high infectivity may instead have emerged via a distinct set of molecular changes in the SARS-Cov2 genome. Second, it calls into question the presumption of a recent zoonotic origin for this disease; while other molecular components of the current SARS-Cov2 virus may have acquired recent evolutionary changes that promoted its infectivity in humans, it appears that the high affinity for hACE2 was not among them.

If this is the case – that this viral lineage possessed the ability to bind hACE2 with high affinity for at least the past 7 years (**Figure 1B**) – then why did it not emerge as a public health issue until recently? One possibility is that binding hACE2 by the Spike-RBD is not sufficient, on its own, to infect humans, and that other molecular components first needed to acquire new functions to do so. A second possibility is that this virus may have been capable of infecting human cells for a longer period of time in the past, but that its ancestral form either presented with far fewer symptoms (making it less disruptive and/or noticeable to those infected), or that it was far less infectious (thereby impacting only a small number of people), in either case escaping the notice of public health monitoring (**Figure 2C**). To test this, a broad and concerted effort to sequence the range of coronaviruses across human populations would need to be conducted, in order to test whether a closely related virus may also be circulating.[43–45]

Naturally, as an *in silico* study, these results should be interpreted with some caution. Insofar as they can be validated, however, they are largely consistent with direct functional measurements in the lab.[42] Ideally, combinatorial libraries could be constructed[46,47] and functionally screened[48] in

order to glean more detailed insights into the molecular mechanisms underlying the recent evolution of this virus.

Predicting the emergence of highly infectious and virulent diseases, while difficult, is vital for human population health.[49] To do so, however, we must take steps to understand how pandemic diseases – such as SARS-Cov2 – emerged as they did, and to understand if and when they acquired the novel molecular functions that enabled their infectivity. In this case, it appears that the SARS-Cov2 Spike-RBD did not recently evolve binding affinity to a human-specific protein. Instead, that function appears to have been latent, making it clear that the evolution of this disease – along with so many other aspects of its etiology – is more complex than expected.

References

1. Parvez, M. K. & Parveen, S. Evolution and Emergence of Pathogenic Viruses: Past, Present, and Future. *Intervirology* **60**, 1-7 (2017).
2. Metcalf, C. J. E. et al. Five challenges in evolution and infectious diseases. *Epidemics* **10**, 40-44 (2015).
3. Kaján, G. L., Doszpoly, A., Tarján, Z. L., Vidovszky, M. Z. & Papp, T. Virus–host coevolution with a focus on animal and human DNA viruses. *Journal of molecular evolution* 1-16 (2019).
4. Huelsenbeck, J. P., Rannala, B. & Yang, Z. Statistical tests of host-parasite cospeciation. *Evolution* **51**, 410-419 (1997).
5. Parrish, C. R. et al. Cross-species virus transmission and the emergence of new epidemic diseases. *Microbiol. Mol. Biol. Rev.* **72**, 457-470 (2008).
6. Brook, C. E. et al. Accelerated viral dynamics in bat cell lines, with implications for zoonotic emergence. *Elife* **9**, e48401 (2020).
7. Saéz, A. M. et al. Investigating the zoonotic origin of the West African Ebola epidemic. *EMBO molecular medicine* **7**, 17-23 (2015).
8. Watanabe, T. & Kawaoka, Y. Pathogenesis of the 1918 pandemic influenza virus. *PLoS pathogens* **7**, (2011).
9. Andersen, K. G., Rambaut, A., Lipkin, W. I., Holmes, E. C. & Garry, R. F. The proximal origin of SARS-CoV-2. *Nature medicine* **26**, 450-452 (2020).
10. Klempner, M. S. & Shapiro, D. S. Crossing the species barrier—one small step to man, one giant leap to mankind. *New England Journal of Medicine* **350**, 1171-1172 (2004).
11. Lu, H., Stratton, C. W. & Tang, Y. W. Outbreak of pneumonia of unknown etiology in Wuhan, China: The mystery and the miracle. *J Med Virol* **92**, 401-402 (2020).
12. Sohrabi, C. et al. World Health Organization declares global emergency: A review of the 2019 novel coronavirus (COVID-19). *Int J Surg* **76**, 71-76 (2020).
13. Gorbalenya, A. E., Enjuanes, L., Ziebuhr, J. & Snijder, E. J. Nidovirales: evolving the largest RNA virus genome. *Virus Res* **117**, 17-37 (2006).
14. Schoeman, D. & Fielding, B. C. Coronavirus envelope protein: current knowledge. *Virol J* **16**, 69 (2019).
15. Joffrin, L. et al. Bat coronavirus phylogeography in the Western Indian Ocean. *Sci Rep* **10**, 6873 (2020).
16. Li, X. et al. Evolutionary history, potential intermediate animal host, and cross-species analyses of SARS-CoV-2. *J Med Virol* **92**, 602-611 (2020).
17. Zhou, P. et al. A pneumonia outbreak associated with a new coronavirus of probable bat origin. *Nature* **579**, 270-273 (2020).
18. Li, C., Yang, Y. & Ren, L. Genetic evolution analysis of 2019 novel coronavirus and coronavirus from other species. *Infect Genet Evol* **82**, 104285 (2020).
19. Lau, S. K. P. et al. Possible Bat Origin of Severe Acute Respiratory Syndrome Coronavirus 2. *Emerg Infect Dis* **26**, (2020).
20. Paraskevis, D. et al. Full-genome evolutionary analysis of the novel corona virus (2019-nCoV) rejects the hypothesis of emergence as a result of a recent recombination event. *Infect Genet Evol* **79**, 104212 (2020).
21. Lam, T. T. et al. Identifying SARS-CoV-2-related coronaviruses in Malayan pangolins. *Nature* (2020).

22. Zhang, T., Wu, Q. & Zhang, Z. Probable Pangolin Origin of SARS-CoV-2 Associated with the COVID-19 Outbreak. *Curr Biol* **30**, 1346-1351.e2 (2020).
23. Li, X. et al. Emergence of SARS-CoV-2 through Recombination and Strong Purifying Selection. *bioRxiv* (2020).
24. Boni, M. F. et al. Evolutionary origins of the SARS-CoV-2 sarbecovirus lineage responsible for the COVID-19 pandemic. *bioRxiv* 2020.03.30.015008 (2020).
25. Belouzard, S., Millet, J. K., Licitra, B. N. & Whittaker, G. R. Mechanisms of coronavirus cell entry mediated by the viral spike protein. *Viruses* **4**, 1011-1033 (2012).
26. Hoffmann, M. et al. SARS-CoV-2 Cell Entry Depends on ACE2 and TMPRSS2 and Is Blocked by a Clinically Proven Protease Inhibitor. *Cell* **181**, 271-280.e8 (2020).
27. Lan, J. et al. Structure of the SARS-CoV-2 spike receptor-binding domain bound to the ACE2 receptor. *Nature* **581**, 215-220 (2020).
28. Donoghue, M. et al. A novel angiotensin-converting enzyme-related carboxypeptidase (ACE2) converts angiotensin I to angiotensin 1-9. *Circ Res* **87**, E1-9 (2000).
29. Walls, A. C. et al. Structure, Function, and Antigenicity of the SARS-CoV-2 Spike Glycoprotein. *Cell* **181**, 281-292.e6 (2020).
30. Ou, X. et al. Characterization of spike glycoprotein of SARS-CoV-2 on virus entry and its immune cross-reactivity with SARS-CoV. *Nat Commun* **11**, 1620 (2020).
31. Stawiski, E. W. et al. Human ACE2 receptor polymorphisms predict SARS-CoV-2 susceptibility. *bioRxiv* 2020.04.07.024752 (2020).
32. Letko, M., Marzi, A. & Munster, V. Functional assessment of cell entry and receptor usage for SARS-CoV-2 and other lineage B betacoronaviruses. *Nat Microbiol* **5**, 562-569 (2020).
33. Becker, M. M. et al. Synthetic recombinant bat SARS-like coronavirus is infectious in cultured cells and in mice. *Proc Natl Acad Sci U S A* **105**, 19944-19949 (2008).
34. Guo, H. et al. Evolutionary arms race between virus and host drives genetic diversity in bat SARS related coronavirus spike genes. *bioRxiv* 2020.05.13.093658 (2020).
35. Forster, P., Forster, L., Renfrew, C. & Forster, M. Phylogenetic network analysis of SARS-CoV-2 genomes. *Proc Natl Acad Sci U S A* **117**, 9241-9243 (2020).
36. Ren, W. et al. Full-length genome sequences of two SARS-like coronaviruses in horseshoe bats and genetic variation analysis. *J Gen Virol* **87**, 3355-3359 (2006).
37. Ou, J. et al. RBD mutations from circulating SARS-CoV-2 strains enhance the structure stability and infectivity of the spike protein. *bioRxiv* 2020.03.15.991844 (2020).
38. Harms, M. J. & Thornton, J. W. Evolutionary biochemistry: revealing the historical and physical causes of protein properties. *Nat Rev Genet* **14**, 559-571 (2013).
39. Wong, M. C., Javornik Cregeen, S. J., Ajami, N. J. & Petrosino, J. F. Evidence of recombination in coronaviruses implicating pangolin origins of nCoV-2019. *bioRxiv* (2020).
40. Kumari, R., Kumar, R., Open, S. D. D. C. & Lynn, A. g_mmpbsa--a GROMACS tool for high-throughput MM-PBSA calculations. *J Chem Inf Model* **54**, 1951-1962 (2014).
41. Baker, N. A., Sept, D., Joseph, S., Holst, M. J. & McCammon, J. A. Electrostatics of nanosystems: application to microtubules and the ribosome. *Proc Natl Acad Sci U S A* **98**, 10037-10041 (2001).
42. Starr, T. N. et al. Deep mutational scanning of SARS-CoV-2 receptor binding domain reveals constraints on folding and ACE2 binding. *bioRxiv* 2020.06.17.157982 (2020).
43. Nsubuga, P. et al. in *Disease Control Priorities in Developing Countries* (eds Jamison, D. T. et al.) (World Bank, Washington (DC), 2006).

44. Wang, N. et al. Serological Evidence of Bat SARS-Related Coronavirus Infection in Humans, China. *Virol Sin* **33**, 104-107 (2018).
45. Li, H. et al. Human-animal interactions and bat coronavirus spillover potential among rural residents in Southern China. *Biosaf Health* **1**, 84-90 (2019).
46. Yang, G. et al. Higher-order epistasis shapes the fitness landscape of a xenobiotic-degrading enzyme. *Nat Chem Biol* **15**, 1120-1128 (2019).
47. Anderson, D. W., McKeown, A. N. & Thornton, J. W. Intermolecular epistasis shaped the function and evolution of an ancient transcription factor and its DNA binding sites. *Elife* **4**, e07864 (2015).
48. Starr, T. N., Picton, L. K. & Thornton, J. W. Alternative evolutionary histories in the sequence space of an ancient protein. *Nature* **549**, 409-413 (2017).
49. Myers, M. F., Rogers, D. J., Cox, J., Flahault, A. & Hay, S. I. Forecasting disease risk for increased epidemic preparedness in public health. *Adv Parasitol* **47**, 309-330 (2000).
50. NCBI, R. C. Database resources of the National Center for Biotechnology Information. *Nucleic Acids Res* **46**, D8-D13 (2018).
51. Katoh, K., Misawa, K., Kuma, K. & Miyata, T. MAFFT: a novel method for rapid multiple sequence alignment based on fast Fourier transform. *Nucleic Acids Res* **30**, 3059-3066 (2002).
52. Katoh, K. & Standley, D. M. MAFFT multiple sequence alignment software version 7: improvements in performance and usability. *Mol Biol Evol* **30**, 772-780 (2013).
53. Guindon, S. & Gascuel, O. A simple, fast, and accurate algorithm to estimate large phylogenies by maximum likelihood. *Syst Biol* **52**, 696-704 (2003).
54. Guindon, S. et al. New algorithms and methods to estimate maximum-likelihood phylogenies: assessing the performance of PhyML 3.0. *Syst Biol* **59**, 307-321 (2010).
55. Letunic, I. & Bork, P. Interactive Tree Of Life (iTOL) v4: recent updates and new developments. *Nucleic Acids Res* **47**, W256-W259 (2019).
56. Altschul, S. F., Gish, W., Miller, W., Myers, E. W. & Lipman, D. J. Basic local alignment search tool. *J Mol Biol* **215**, 403-410 (1990).
57. Shu, Y. & McCauley, J. GISAID: Global initiative on sharing all influenza data - from vision to reality. *Euro Surveill* **22**, (2017).
58. Elbe, S. & Buckland-Merrett, G. Data, disease and diplomacy: GISAID's innovative contribution to global health. *Glob Chall* **1**, 33-46 (2017).
59. Yachdav, G. et al. MSAViewer: interactive JavaScript visualization of multiple sequence alignments. *Bioinformatics* **32**, 3501-3503 (2016).
60. Edgar, R. C. MUSCLE: multiple sequence alignment with high accuracy and high throughput. *Nucleic Acids Res* **32**, 1792-1797 (2004).
61. Darriba, D., Taboada, G. L., Doallo, R. & Posada, D. ProtTest 3: fast selection of best-fit models of protein evolution. *Bioinformatics* **27**, 1164-1165 (2011).
62. Le, S. Q. & Gascuel, O. An improved general amino acid replacement matrix. *Mol Biol Evol* **25**, 1307-1320 (2008).
63. Stamatakis, A. RAxML version 8: a tool for phylogenetic analysis and post-analysis of large phylogenies. *Bioinformatics* **30**, 1312-1313 (2014).
64. Ashkenazy, H. et al. FastML: a web server for probabilistic reconstruction of ancestral sequences. *Nucleic Acids Res* **40**, W580-4 (2012).

65. Foley, G. et al. Identifying and engineering ancient variants of enzymes using Graphical Representation of Ancestral Sequence Predictions (GRASP). *bioRxiv* 2019.12.30.891457 (2020).
66. Schrödinger, L. L. C. The PyMOL Molecular Graphics System. **Version 1.2r3pre,**
67. Duan, Y. et al. A point-charge force field for molecular mechanics simulations of proteins based on condensed-phase quantum mechanical calculations. *J Comput Chem* **24**, 1999-2012 (2003).
68. Humphrey, W., Dalke, A. & Schulten, K. VMD: visual molecular dynamics. *J Mol Graph* **14**, 33-8, 27 (1996).

Supplementary Methods

Confirmation of SARS-CoV-2 genome evolution

A phylogenetic analysis of 26 viral genomes was performed to confirm known SARS_CoV_2 ancestors. 24 known enzootic and endemic viruses and the SARS-CoV-2 reference genome and the Pangolin-CoV genome were downloaded from the National Center for Biotechnology Information (NCBI)[50] and Lam et al.[21] respectfully. Selected sequences were aligned using the Multiple Alignment using Fast Fourier Transform Version 7 (MAFFT) FFT-NS-2 algorithm. [51,52] MAFFT default parameters were used in our alignment, meaning gap penalties were assigned a value of 1.53. PhyML 3.0 was employed to construct a phylogeny of aligned genomes. [53,54] Bayes values ≥ 0.90 were considered statistically significant. The output tree was visualized using the online tool, Interactive Tree of Life (iTOL), and statistically significant clades were examined to validate current knowledge surrounding SARS-CoV-2 evolution.[55]

We isolated the RbRp domain from the SARS-CoV-2 reference genome using the Basic Local Alignment Search Tool (BLAST).[56] First, we performed a tblastn search of the SARS-CoV-2 RbRp reference domain published on NCBI using a BLOSUM 62 matrix, a gap opening penalty of 11 and a gap extension penalty of 1.[50] We then used the output of this query to find the specific location of the RbRp domain in the nucleotide SARS-CoV-2 reference genome and isolated this portion of the genome for our analysis. Next, we employed BLASTn to isolate the RbRp domain from the pangolin coronavirus and the RaTG13 coronavirus. In this alignment, we used the gap opening penalty of 0 and gap extension penalty of 2.5. We also downloaded the 127 RbRp bat coronavirus sequences published by Joffrin et al.[15] Isolated RbRp sequences were aligned using the MAFFT G-INS-I algorithm.[51,52] Gap opening and extension penalties were the same as previously described. Finally, we created a phylogeny of the aligned sequences using PhyML 3.0. [53,54] The tree was visualized using iTOL and statistically significant clades were examined.[55]

Identification of geographic differences in SARS-CoV-2 sequences

To identify geographic and time dependent differences in the SARS-CoV-2 viral genome, we performed a phylogenetic analysis of 479 SARS-CoV-2 sequences obtained from GISAID (**Supplementary Table 3**).[57,58] We arbitrarily selected one sequence per day per country from December 30, 2019 to March 25, 2020. We also included the RaTG13 reference genome and the Pangolin-CoV genome published by Lam et al. in our analysis. [21,50] Selected sequences were aligned, as previously described, using the MAFFT FFT-NS-2 alignment algorithm.[51,52] A consensus sequence was constructed from the 479 aligned SARS-CoV-2 sequences using the online tool MSAViewer.[59] We validated our consensus sequence by cross referencing the sequence to the SARS-CoV-2 reference genome published by NCBI.[50] Following, validation we uploaded the consensus sequence to the online cloud-based informatics platform, Benchling, and extracted the ORFs (benchling.com).

To determine common SNPs within the 479 SARS-CoV-2 sequences, the consensus ORFs were aligned using Nucleotide BLAST.[56] By default, our analysis used a gap opening penalty of 5, a gap extension penalty of 2 and a mismatch penalty of -3. SNPs were extracted from the BLAST output using the Java module BlastNToSnp (http://dx.doi.org/10.6084/m9.figshare.1425030). We then selected for SNPs present in >5% of the sequences and inputted the SNPs into Benchling to determine whether the SNPs caused silent or missense mutations in the ORFs (benchling.com).

PhyML 3.0 was employed to construct a phylogenetic tree of the 479 aligned SARS-CoV-2 genomes, the RaTG13 genome and the Pangolin-CoV genome, [53,54] which was visualized using iTOL.[55]

Ancestral sequence reconstruction of spike glycoprotein receptor binding domain:

nBLASTx, run using a BLOSUM 62 matrix, a gap opening penalty of 11 and a gap extension penalty of 1, was employed to extract the Spike glycoprotein from the 479 SARS-CoV-2 sequences and the Pangolin-CoV genome.[56] Additional, Spike sequences, including the RaTG13 Spike protein, were obtained directly from NCBI.[50] Protein sequences were initially aligned using the Multiple Sequence Alignment by Log-Expectation (MUSCLE) program.[60] The optimal parameters for phylogenetic reconstruction analysis were taken from the best-fit evolutionary model selected using the Akaike Information Criterion (AIC) implemented in the PROTTEST3 software,[61] and were inferred to be the Jones-Taylor-Thornton (JTT) model[62] with gamma-distributed among-site rate variation and empirical state frequencies. Phylogeny was inferred from these alignments using the RaXML v8.2.9 software[63] and results were visualized using FigTree v1.4.4 (https://github.com/rambaut/figtree/releases). Ancestral sequence reconstruction was performed with the FastML software[64] and further validated independently using the Graphical Representation of Ancestral Sequence Predictions (GRASP) software.[65] Statistical confidence in each position's reconstructed state for each ancestor determined from posterior probability. For the N1 ancestor, all RBD positions had very high reconstructed probability (>0.95). For the N0 ancestor, there were only one "ambiguous" position in the RBD (defined as PP < 0.85), which was identified and discussed extensively in the text (as the most probable state was different than the N1 ancestor).

Mutagenesis of ancestral proteins:

To understand the evolutionary importance of sequence changes observed between ancestral, zoonotic, and SARS-CoV-2 spike protein sequences, *in silico* mutagenesis and binding energy studies were performed. A previously constructed x-ray crystallography structure for the complex between the receptor binding domain (RBD) of the SARS-CoV-2 spike protein and the human hACE2 receptor were obtained from RCSB (accession number 6M0J). Utilizing PyMOL mutagenesis wizard, [66] the four missense mutations (R346t, A372t, Q498h or Q498y, H519n) identified between the N0 and N1 sequences were introduced into the SARS-CoV-2 RBD sequence, replicating the sequence of the putative ancestral zoonotic (N0) sequence. In addition to the N1 and N0 structures, additional structures were developed in a similar fashion, selectively including each of the 4 mutations to represent all of the possible combinations that these mutations may have existed throughout evolutionary time

Molecular dynamics simulation of Spike-RBD-hACE2 interactions:

Molecular interactions were characterized with molecular dynamics simulations using Gromacs, TIP3P waters and CHARM07 force-field parameters for proteins. For each condition, three replicate 10 ns simulations were run, starting from crystal structures or structural models. Historical mutations were introduced and energy-minimized before MD simulation. Each system

was solvated in a cubic box with a 10 Å margin, then neutralized and brought to 150 mM ionic strength with sodium and chloride ions. This was followed by energy minimization to remove clashes, assignment of initial velocities from a Maxwell distribution, and 1 ns of solvent equilibration in which the positions of heavy protein and DNA atoms were restrained. Production runs were 50 ns, with the initial 10 ns excluded as burn-in. The trajectory time step was 2 fs, and final analyses were performed on frames taken every 12.5 ps. We used TIP3P waters and the CHARM07 FF03 parameters for proteins, as implemented in GROMACS 4.5.5.[67] Analyses were performed using VMD 1.9.1.[68] GROMACS output was uploaded into Visual Molecular Dynamics (VMD) for Root-Mean Squared Deviation (RMSD) Analysis using the RMSD trajectory tool. We noted consistently large RMSD values for the full RBD (i.e. including the regions distant from the binding interface), and so we limited our analysis to residues 397 to 512 of the RBD (i.e. the region shown to make contact with hACE2, and maintain stable RMSD across all simulations).

Measurement of binding energies:

Next, we measured the binding energies between residues 397 to 512 and the ACE2 receptor using g_mmpbsa, a program which employs Molecular mechanics Poisson–Boltzmann surface area (MMPBSA) calculations to determine binding energy. Van der Waal forces, polar solvation energy, apolar solvation energy and SASA energy were calculated every 0.25 ns using a gridspace of 0.5 and a solute dielectric constant of 2. The output of the three replicates was amalgamated and binding energy was calculated using the bootstrap analysis (n = 2000 bootstraps) published by Kumari et al.[40,41] We then characterize the genetic effect of each mutation (on average) and assessed whether there were any statistically significant epistatic interactions using established methods.[46,47]

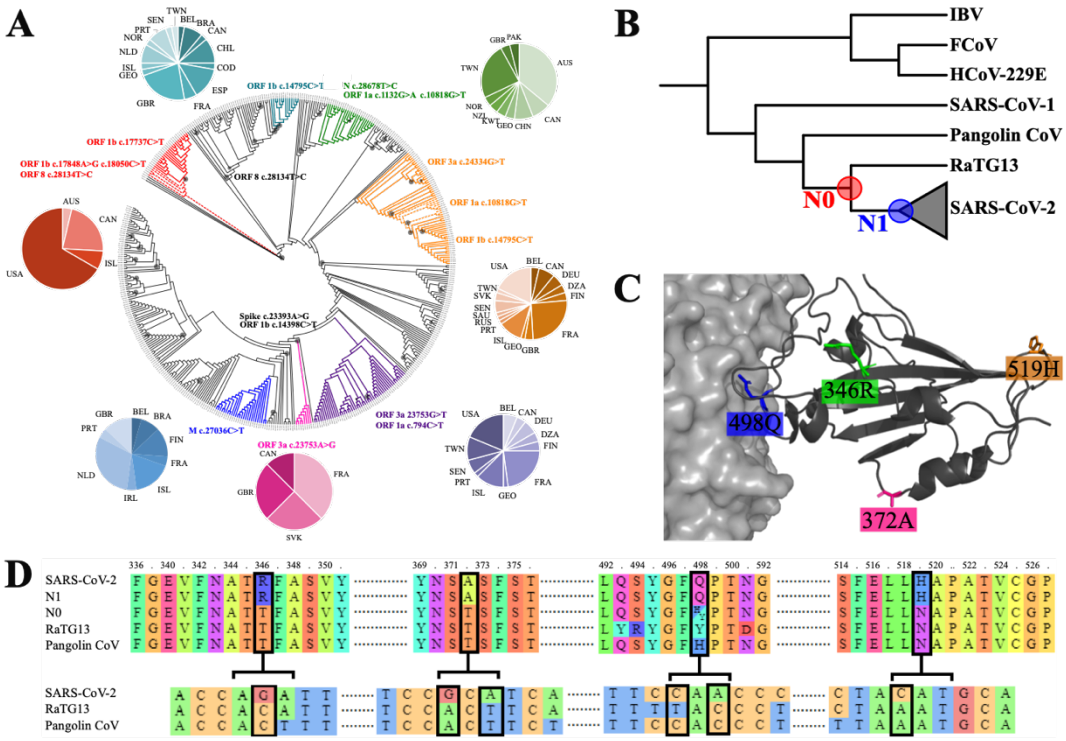

Figure 1: Detailed examination of SARS-CoV-2 evolution. A. Cladogram illustrating location-dependent evolution of the SARS-CoV-2 full genome following viral infection (December 30, 2019 - March 20, 2020). Distinct mutations (present in >5% of the examined sequences) are coloured and statistically significant clades (Bayes value > 0.9) are highlighted with black circles. **B.** Cladogram illustrating the last common ancestor all SARS-CoV-2 Spike-RBDs (N1) and of SARS-CoV-2 and the RaTG13 Spike-RBD (N0). **C.** Structural representation of the four mutations in the Spike-RBD (ribbon diagram) relative to the ACE2 receptor (Space filling model) that differ between N0 to N1. Stick models show the mutations in their N1 state. **D.** Alignment of the of the Spike-RBD of SARS-CoV-2 and its ancestors for both protein (top) and DNA (bottom). Black boxes highlight the four mutations that differ from N0 to N1.

A

	Mutations				MM/PBSA Complex Energy (SEM)	
	t346R	t372A	h/y 498Q	n519H		
N0					-283.592 (8.275)	-253.46 (13.537)
346	X				-246.821 (4.482)	-257.93 (13.083)
372		X			-244.057 (11.594)	-250.372 (6.540)
498			X		-237.694 (10.064)	
519				X	-240.533 (9.760)	-229.712 (10.455)
346_372	X	X			-228.431 (14.036)	-312.755 (11.75)
346_498	X		X		-251.783 (11.709)	
346_519	X			X	-215.702 (12.883)	-277.341 (11.983)
372_498		X	X		-71.773 (12.868)	
372_519		X		X	-260.865 (7.922)	-245.856 (12.283)
498_519			X	X	-237.61 (12.145)	
346_372_498	X	X	X		-215.836 (44.957)	
346_372_519	X	X		X	-217.909 (60.249)	-162.627 (18.346)
372_498_519		X	X	X	-197.788 (13.872)	
346_498_519	X		X	X	-229.043 (13.394)	
N1	X	X	X	X	-143.6 (33.398)	

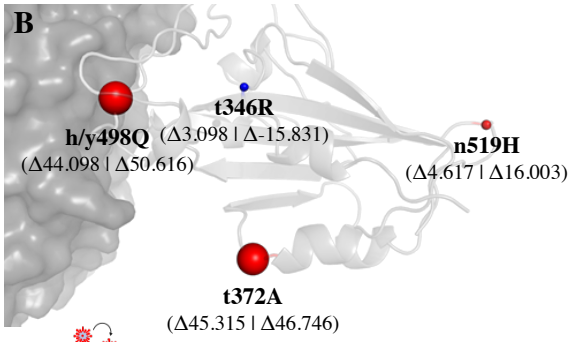

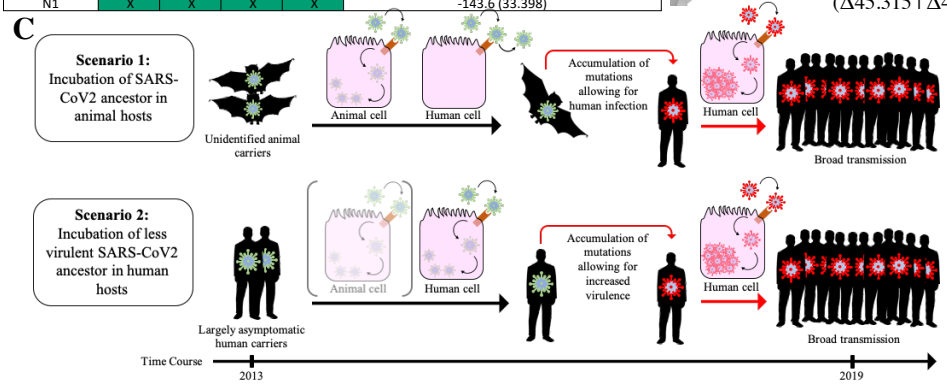

Figure 2: Characterization of SARS-CoV-2 Spike-RBD functional evolution. A. Table of MM/PBSA binding energies between receptor binding domains of SARS-CoV2 evolutionary constructs and hACE2 receptor (note that lower energy indicates tighter binding). Blue cells indicate the presence of the ancestral (N0) state and green cells (with an "x") indicate the presence of the SARS-CoV-2 state (N1) at a given position. Two values are present for constructs with an ancestral (N0) state at position 498 (which reflect the ambiguity of its ancestral reconstruction), corresponding to h498 and y498 from left to right. Energies are shown as the mean of three replicate simulations with SEM indicated in parenthesis. **B.** Relative effect of changes in SARS-CoV-2 receptor binding domain from ancestral (N0) to SARS-CoV-2 (N1) state on MM/PBSA binding energies. Size of spheres indicate the relative magnitude, with red spheres indicating decreased binding affinity and blue indicating increased binding affinity. Values are averaged for h498 and y498 states (both raw values shown in parentheses). **C.** Schematic of two possible evolutionary scenarios stemming from the observed evolutionary SARS-CoV-2 Spike-RBD function. In Scenario 1, it is postulated that a zoonotic ancestral SARS-CoV-2 strain possessed the ability to effectively bind hACE2 but was unable to effectively enter human cells, requiring the presence of subsequent mutations to infect humans. In Scenario 2, an ancestral SARS-CoV-2 strain was actively infecting humans prior to the outbreak at low levels, thus escaping public health detection until subsequent mutations lead to increased infectivity and/or severity.

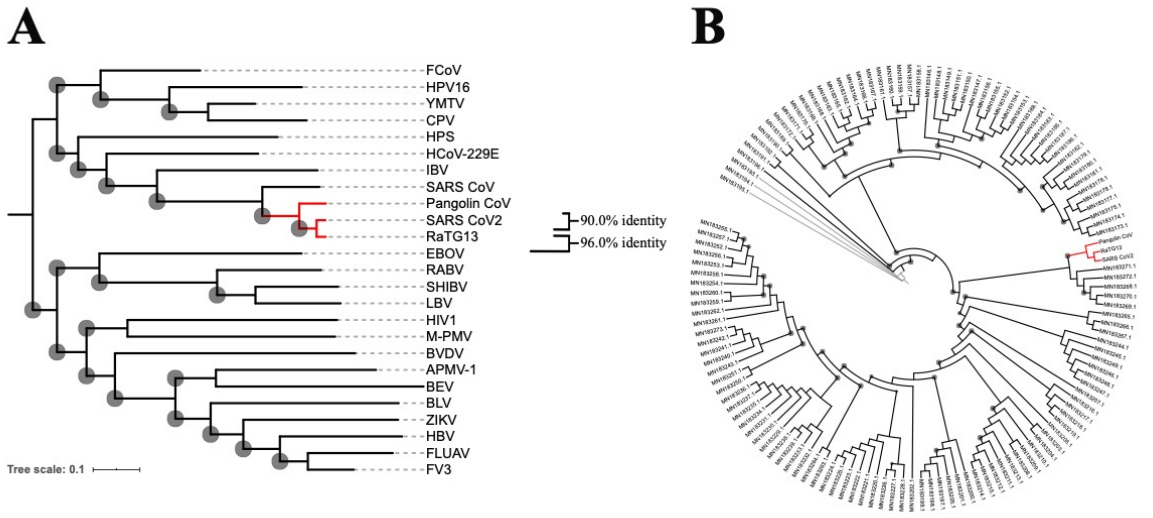

Supplementary Figure 1: Phylogenetic reconstruction of family that includes SARS-CoV-2. Phylogenies were constructed using whole genome sequencing data from a series of known coronaviruses. The two closest relatives to SARS-CoV-2 are highlighted in red and sequence identities are specified. **A.** Displays phylogeny of 25 whole genomes of related coronaviruses represented as a horizontal cladogram, with sequence identities compared to RaTG13 and Pangolin CoV genomes specified. **B.** Phylogenetic reconstruction of 127 RdRp sequences represented as a circular cladogram, including a larger number of related coronavirus sequences.

N0 (with 498H)

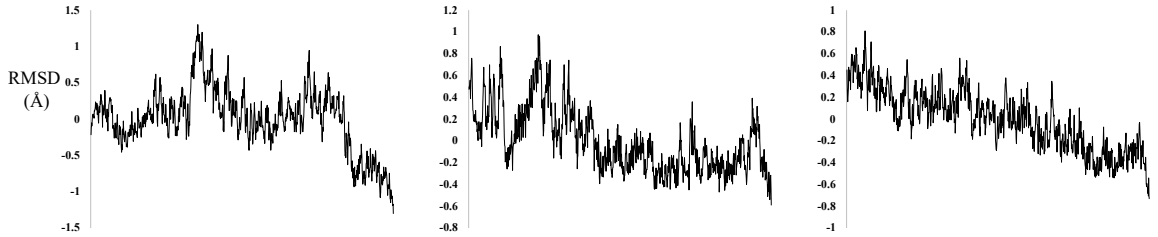

N0 (with 498Y)

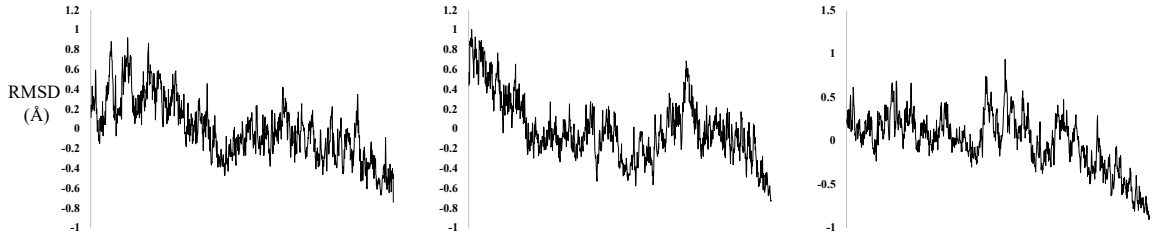

346 (with 498H)

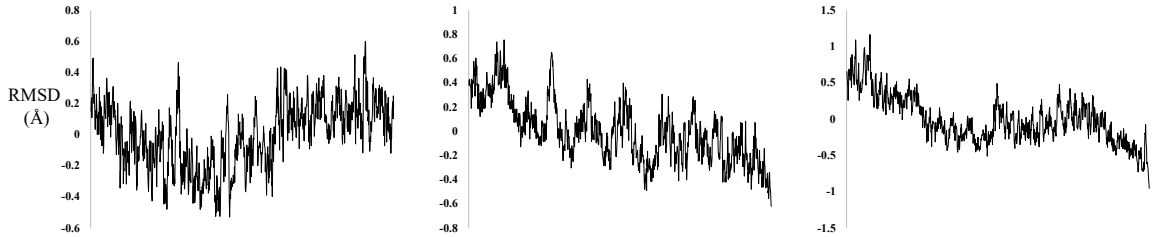

346 (with 498Y)

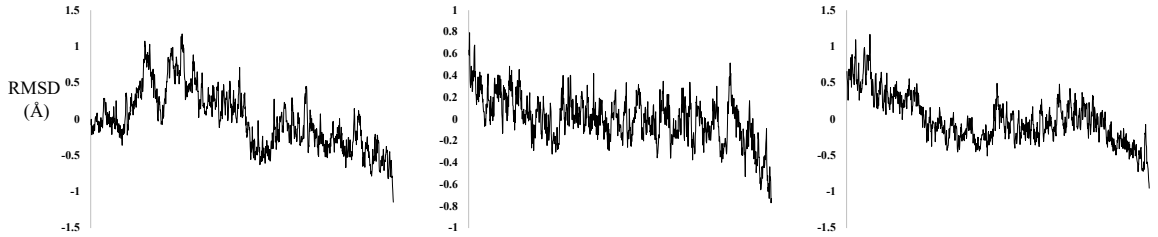

372 (with 498H)

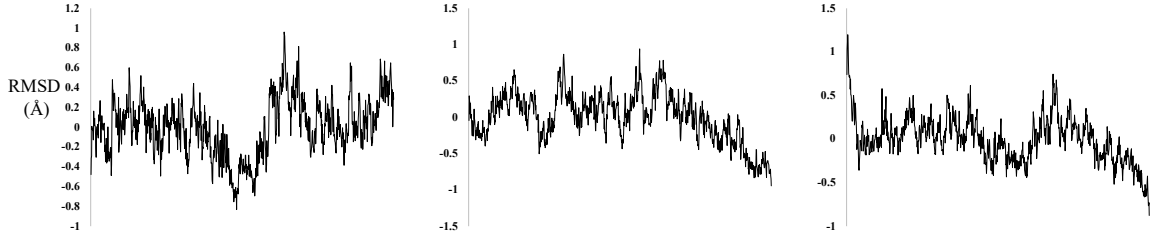

346 372 (with 498Y)

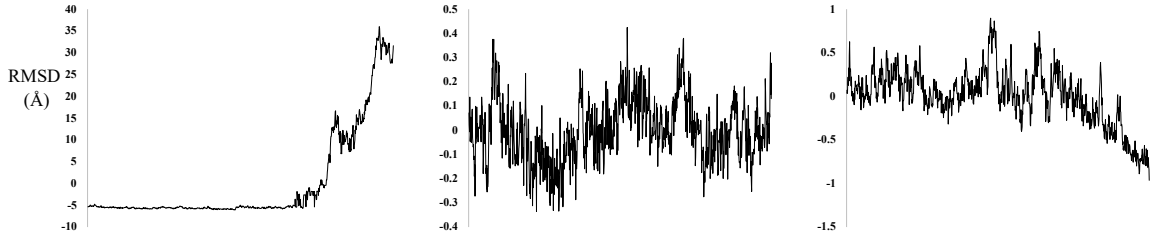

346 498

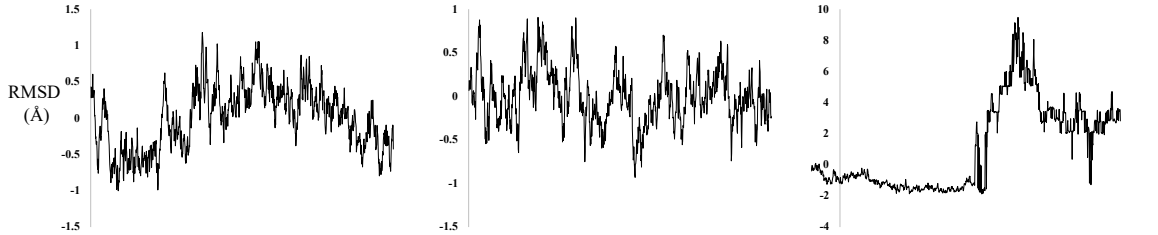

346 519 (with 498H)

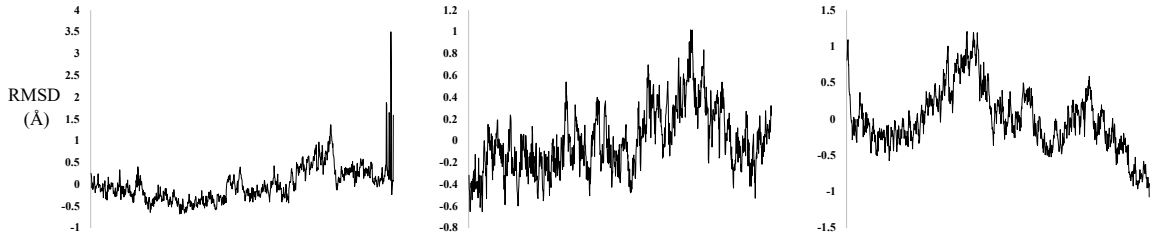

346 519 (with 498Y)

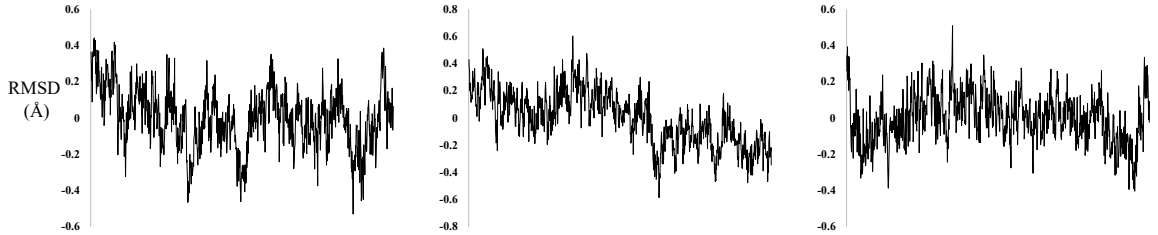

372 498

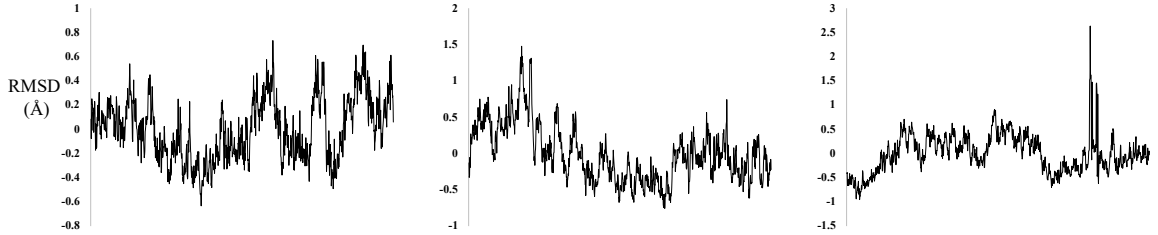

372 (with 498Y)

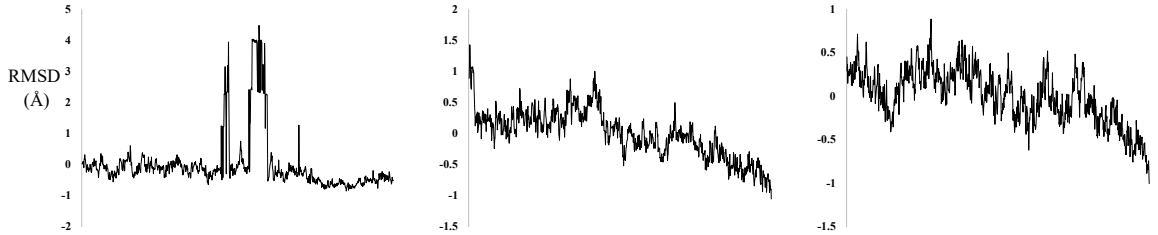

498

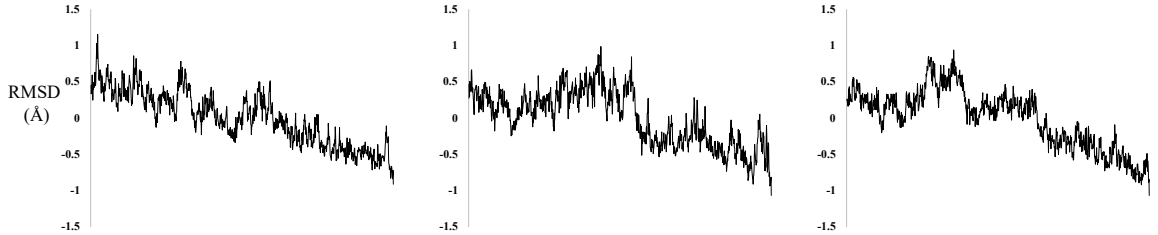

519 (with 498H)

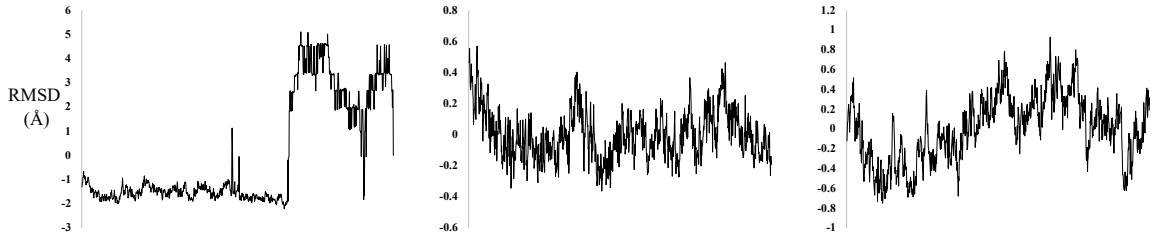

519 (with 498Y)

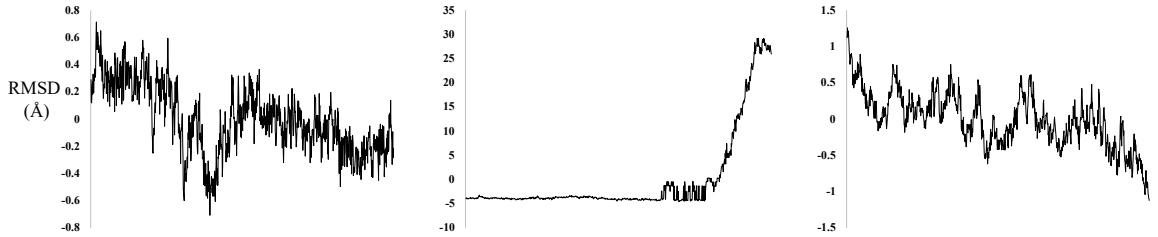

346 372 (with 498H)

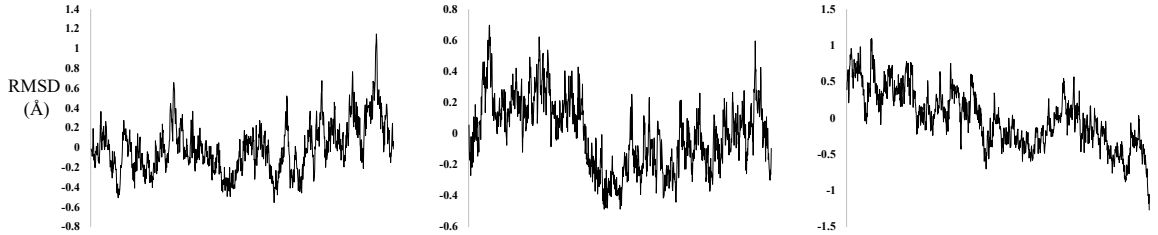

:

372 519 (with 498H)

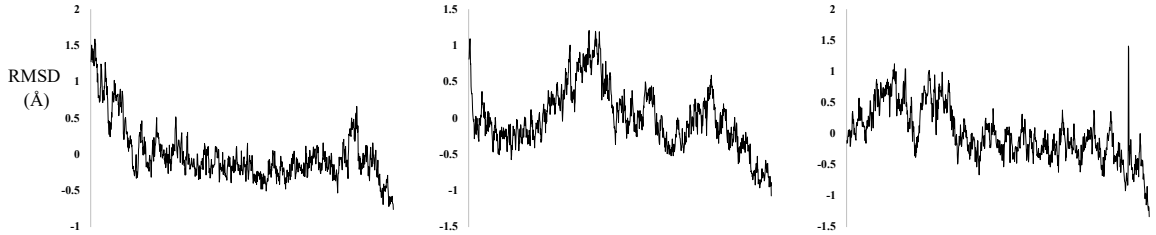

372 519 (with 498Y)

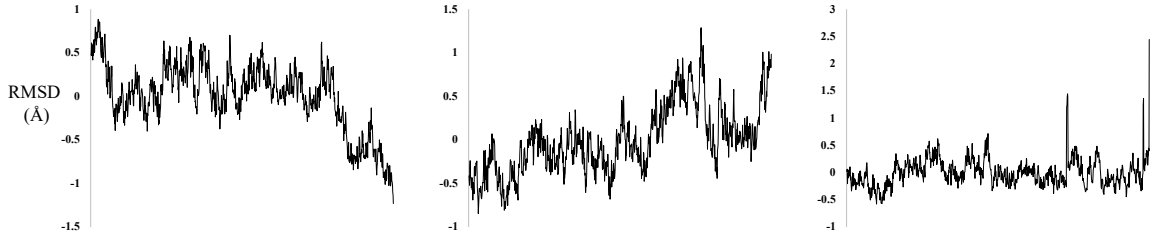

498 519

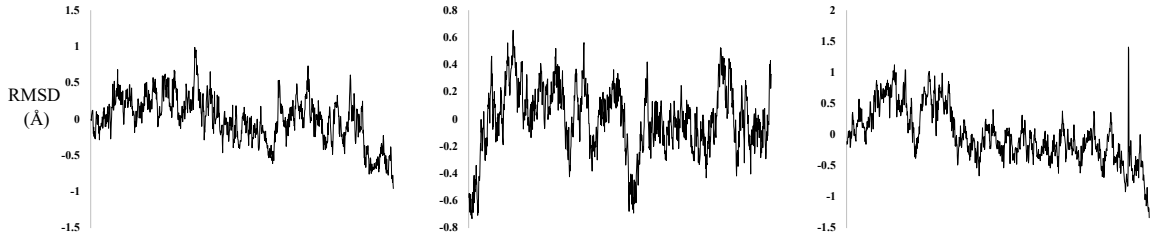

346 372 498

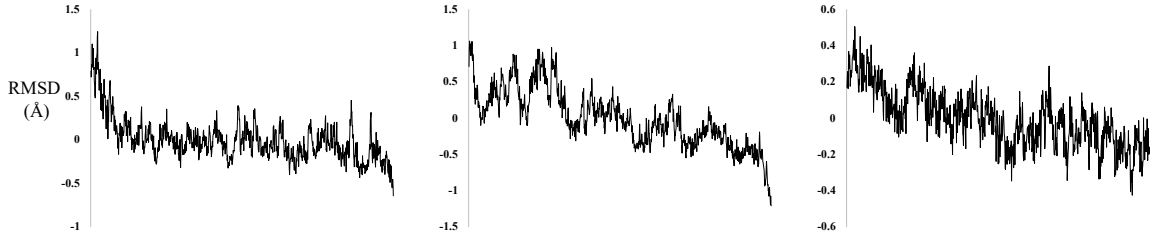

346 372 519 (with 498H)

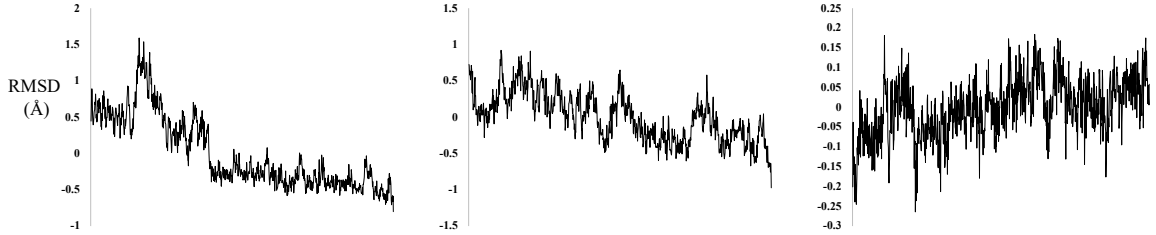

346 372 519 (with 498Y)

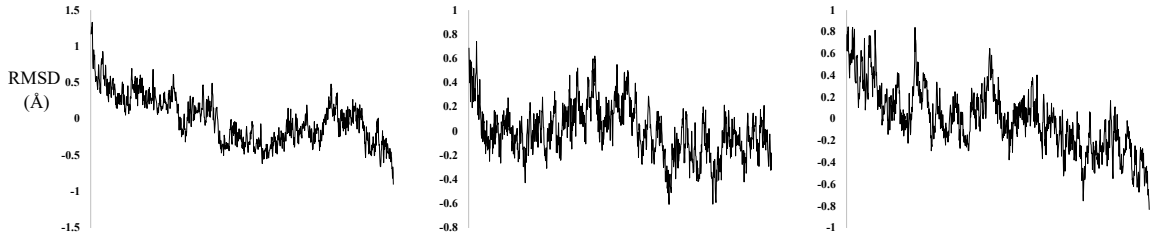

346 498 519

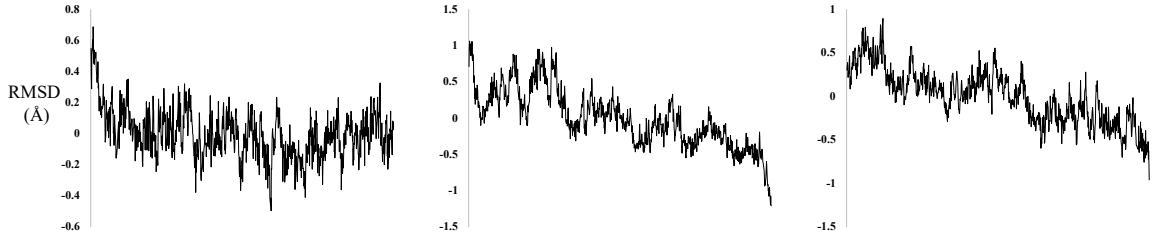

N1

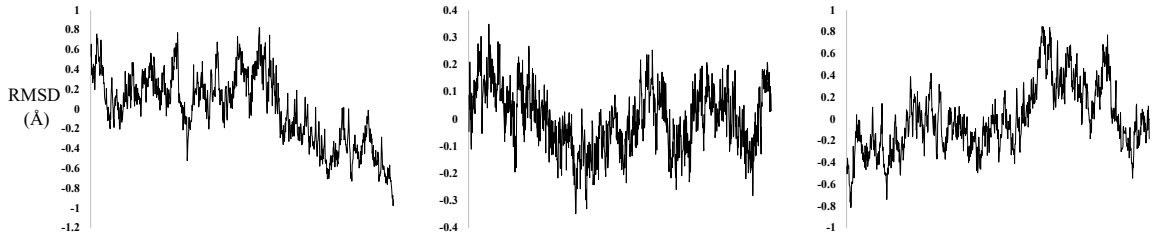

Supplementary Figure 2: RMSD of simulation data used for energy calculations. Root-mean-square deviation (RMSD) is shown for simulation window that was used to calculate complex binding energy. Note that the Spike-RBD maintains a consistent stable configuration at the interface with hACE2, suggesting our energy calculations can be safely compared across simulations and that higher random stochasticity should not be a confounding factor.

ORF	Position	Number of Sequences		SNP	Mutation Type
		Raw Count	Percentage		
1a	794	52	10.9	C>T	Missense
	1132	25	5.22	G>A	Missense
	2772	216	45.1	C>T	Silent
	8517	95	19.8	C>T	Silent
	10818	77	16.1	G>T	Missense
1b	14398	215	44.9	C>T	Missense
	14795	38	7.93	C>T	Silent
	17737	24	5.01	C>T	Missense
	17848	28	5.84	A>G	Missense
	18050	30	6.26	C>T	Silent
S	23393	215	44.9	A>G	Missense
3a	23753	61	12.7	G>T	Missense
	24334	59	12.3	G>T	Missense
M	27036	24	5.01	C>T	Missense
8	28134	91	19.0	T>C	Missense
N	28678	25	5.22	T>C	Silent

Supplementary Table 1: Frequency of genomic variants across SARS-CoV-2 infections. Each noted variant that differs from the SARS-CoV-2 reference genome sequence is compiled, counted, and its frequency across human infections measured here is indicated, as well as the type of polymorphism and its potential impact on a protein-coding sequence.

	FastML reconstructions				GRASP reconstructions			
Position	N0	Confidence	N1	Confidence	N0	Confidence	N1	Confidence
346	T	0.94	R	1	T	0.99	R	1
372	T	0.97	A	1	T	0.91	A	1
498	H/Y	0.3/0.61	Q	1	H/Y	0.48/0.40	Q	1
519	N	0.98	H	1	N	0.94	H	1

Supplementary Table 2: Statistical confidence of ancestral sequence reconstructions for positions that vary between N0 and N1. Ancestral sequence reconstruction was assessed via computed posterior probability for each reconstructed state at each position in the sequence. The posterior probability for each reconstructed state at the four key positions that vary between N0 and N1 is shown, as calculated by two independent software packages (FastML and GRASP).

	Number of Sequences				Average Age of Sequenced Patients			
Country	Male	Female	Unknown	All	Male	Female	Unknown	All
Algeria	1	1	0	2	97.0	28.0	N/A	62.5
Australia	11	15	1	27	38.5	36.0	N/A	37.1
Belgium	14	9	0	23	40.6	54.2	N/A	45.9
Brazil	5	3	0	8	37.0	29.0	N/A	34.0
Cambodia	1	0	0	1	60.0	N/A	N/A	60.0
Canada	10	7	0	17	64.5	54.7	N/A	60.5
Chile	4	3	0	7	30.5	43.0	N/A	35.9
China	29	7	7	43	48.9	47.7	N/A	48.7
Congo	3	2	0	5	45.0	28.5	N/A	38.4
Czech Rep	1	0	0	1	44.0	N/A	N/A	44.0
Denmark	4	1	0	5	40.5	21.0	N/A	36.6
Finland	4	4	0	8	67.3	38.3	N/A	52.8
France	17	11	3	31	62.0	63.2	56.0	61.8
Georgia	8	2	0	10	39.9	40.0	N/A	39.9
Germany	1	1	9	11	N/A	38.0	N/A	38.0
Greece	0	0	1	1	N/A	N/A	N/A	N/A
Hong Kong	10	11	0	21	57.3	51.3	N/A	54.1
Hungary	2	1	0	3	26.5	26.0	N/A	26.3
Iceland	5	13	0	18	44.4	46.8	N/A	46.1
India	1	0	0	1	23.0	N/A	N/A	23.0
Ireland	2	2	0	4	54.0	25.5	N/A	39.8
Italy	9	2	0	11	56.0	72.5	N/A	59.0
Japan	1	2	8	11	60.0	62.0	N/A	61.3
Kuwait	0	0	1	1	N/A	N/A	N/A	N/A
Luxembourg	0	1	1	2	N/A	32.0	N/A	32.0
Malaysia	1	2	0	3	11.0	40.0	N/A	30.3
Mexico	1	0	0	1	35.0	N/A	N/A	35.0
Nepal	1	0	0	1	32.0	N/A	N/A	32.0
Netherlands	0	0	14	14	N/A	N/A	N/A	N/A
New Zealand	1	2	0	3	N/A	60.0	N/A	60.0
Norway	0	0	6	6	N/A	N/A	N/A	N/A
Pakistan	0	1	0	1	N/A	40.0	N/A	40.0
Panama	0	1	0	1	N/A	40.0	N/A	40.0
Peru	0	1	0	1	N/A	61.0	N/A	61.0
Poland	1	0	0	1	66.0	N/A	N/A	66.0
Portugal	10	4	1	15	32.3	34.5	N/A	33.1
Russia	0	1	0	1	N/A	30.0	N/A	30.0
Saudi Arabia	1	1	0	2	68.0	67.0	N/A	67.5
Senegal	5	2	0	7	44.4	55.0	N/A	47.4
Singapore	8	4	0	12	45.7	44.5	N/A	45.2
Slovakia	1	1	0	2	26.0	59.0	N/A	42.5
South Africa	1	0	0	1	38.0	N/A	N/A	38.0
South Korea	4	0	2	6	46.3	N/A	N/A	46.3
Spain	13	3	0	16	61.5	47.7	N/A	58.9
Sweden	0	0	1	1	N/A	N/A	N/A	N/A
Switzerland	2	0	9	11	49.0	N/A	50.2	50.0
Taiwan	4	10	0	14	52.0	56.2	N/A	55.0
Thailand	0	1	0	1	N/A	74.0	N/A	74.0
UK	17	12	0	29	55.2	50.6	N/A	53.4
USA	7	8	38	53	38.7	52.0	N/A	45.8
Vietnam	1	2	1	4	50.0	57.0	N/A	54.7
All Countries	222	154	103	479	49.1	47.8	51.7	48.7

Supplementary Table 3: Sources of all SARS-CoV-2 genome sequences. Each genome sequence analyzed from SARS-CoV-2 infection cases are detailed according to geographic region of origin, as well as potentially relevant patient meta-data.